The sensitive magnetoimpedance effect in Fe-based soft ferromagnetic ribbons

1997 J. Phys.: Condens. Matter 9 7269

(http://iopscience.iop.org/0953-8984/9/35/002)

J. Phys.: Condens. Matter **9** (1997) 7269–7280. Printed in the UK PII: S0953-8984(97)82295-3

The sensitive magnetoimpedance effect in Fe-based soft ferromagnetic ribbons

C Chen†‡, L M Mei†, H Q Guo‡, K Z Luan†, Y H Liu†, B G Shen‡ and J G Zhao‡

† Department of Physics, Shandong University, Jinan 250100, People's Republic of China
‡ State Key Laboratory of Magnetism, Institute of Physics and Centre for Condensed Matter Physics, Chinese Academy of Sciences, Beijing 100080, People's Republic of China

Received 4 March 1997, in final form 13 May 1997

Abstract. A comprehensive analysis of magnetoimpedance (MI) phenomena in Fe-based nanocrystalline ribbons is presented in this paper. Giant MI responses have been observed in nanocrystalline samples annealed over the temperature range 490 and 600 °C. More than 400% increases of the MI ratio were obtained both in $Fe_{73.5}CuNb_3Si_{13.5}B_9$ and in $Fe_{88}Zr_7B_4Cu$ ribbons. The sensitivity can reach a value larger than 60% Oe^{-1} in the field range 3–7.2 Oe at 800 kHz for $Fe_{73.5}CuNb_3Si_{13.5}B_9$ ribbons. No MI effect was observed in an as-quenched amorphous $Fe_{88}Zr_7B_4Cu$ sample, because of its very low permeability. A mostly resistive feature was found in an as-quenched amorphous $Fe_{73.5}CuNb_3Si_{13.5}B_9$ sample. The field dependences of the effective permeability show a typical transverse anisotropy property, and the development of the transverse anisotropy in naturally annealed Fe-based ribbons was analysed.

1. Introduction

Recently, giant magnetoimpedance (GMI) effects have been observed in soft ferromagnets [1–15]. The large magnitude of the MI effect, together with a very high sensitivity at low fields, have prompted consideration of potential applications in field-sensing and magnetic recording heads. Most reports concerning magnetoimpedance until now have been related to Co-based amorphous wires [1–11] or ribbons [3, 11–13], which have very high permeability and slightly negative magnetostriction, of the order of -10^{-7}. After annealing under tensile stress or a transverse magnetic field, a circumferential (in the case of a wire) or transverse (in the case of a ribbon) anisotropy, accompanied by corresponding domain structure, was formed, which is believed to be crucial to the GMI effect. It was suggested that the small negative magnetostriction and the large magnetic permeability in the as-quenched state of Co-based alloys constitute the basis of the transverse magnetic anisotropy obtained through appropriate annealing.

Both $Fe_{73.5}CuNb_3Si_{13.5}B_9$ and $Fe_{88}Zr_7B_4Cu$ ribbons are well known soft ferromagnets in their nanocrystalline states, having high permeability and a relatively large magnetostriction. The purpose of our work is to investigate whether GMI effects can arise from soft ferromagnets with microcrystalline or nanocrystalline structures, and whether they exist for soft ferromagnets with small positive magnetostriction constants. In this paper, the GMI effects in both of the types of nanocrystalline ribbon will be reported. The frequency and magnetic field dependence of their MI were studied in detail. The results are very promising.

0953-8984/97/357269+12$19.50

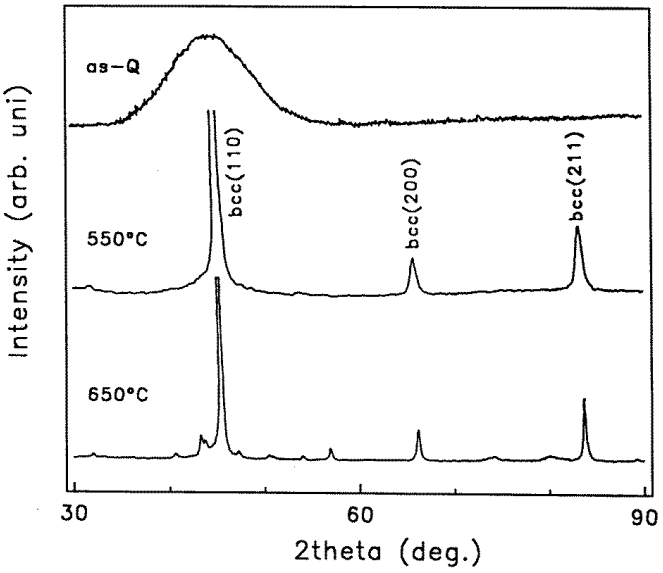

Figure 1. X-ray diffraction patterns for as-quenched and annealed $Fe_{73.5}CuNb_3Si_{13.5}B_9$ ribbons.

2. Experimental details

The materials were prepared in an argon atmosphere by a single-roller melt-quenching method. The ribbons obtained, about 20–30 μm thick, were cut to lengths of several centimetres, and annealed naturally in an oven, without applying a magnetic field. The oven was evacuated to a pressure of the order of 10^{-5} Torr. Three groups of samples were studied in this report.

(I) $Fe_{73.5}CuNb_3Si_{13.5}B_9$ ribbons 10 mm in width and 40 mm in length were annealed at a chosen temperature between 350 and 650 °C . After the temperature had been kept fixed for 15 minutes, the sample was pulled out of the oven and cooled naturally in the vacuum system.

(II) $Fe_{73.5}CuNb_3Si_{13.5}B_9$ ribbons 10 mm in width and 40 mm in length, kindly provided by the Institute of Physics of the Slovak Academy of Sciences in Bratislava, were annealed at 550 °C for times ranging from 0.5 to 18 hours in order to vary the size of the nanocrystals.

(III) $Fe_{88}Zr_7B_4Cu$ ribbons 1.2 mm in width and 30 mm in length were annealed for one hour at various temperatures ranging from 350 to 650 °C, and then cooled naturally in the vacuum system.

All of the data presented here were obtained by using an HP4192A impedance analyser. The leads, made of the metal In, were attached to the ribbons. The contact resistance was less than 1 W. The samples were connected to the analyser with the accessory 16048B test lead, which is a carefully designed item of equipment comprising four coaxial cables. The cables were 100 cm long, and permitted the ribbons to be placed within a Helmholtz coil (diameter 30 cm), which produced a dc magnetic field in the range -75 Oe $\leqslant H \leqslant 75$ Oe. The applied dc field was parallel to the alternating current. The drive current amplitude used was 10 mA. All of the data were collected at room temperature.

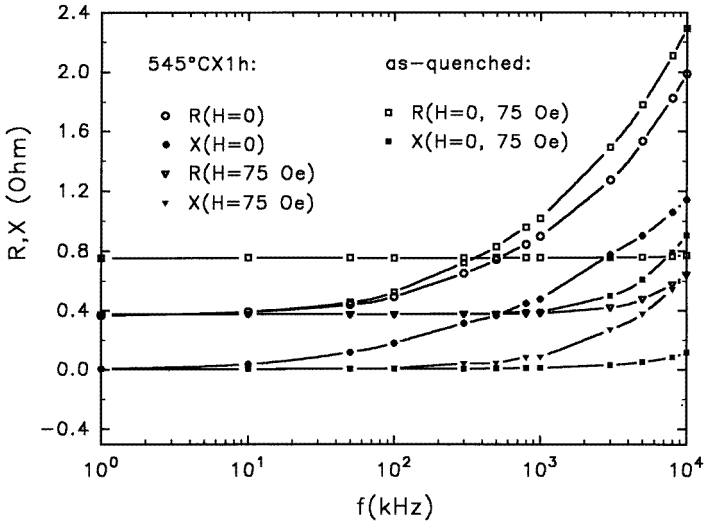

Figure 2. The dependence of the resistance R and the reactance X on the drive ac frequency f for $Fe_{88}Zr_7B_4Cu$ ribbon samples annealed for 1 h at 545 °C, and the as-quenched samples, with zero applied dc field and a field of 75 Oe in the longitudinal direction.

3. Results and discussion

3.1. X-ray diffraction

X-ray diffraction has confirmed that the crystallizing temperatures for $Fe_{73.5}CuNb_3Si_{13.5}B_9$ and $Fe_{88}Zr_7B_4Cu$ are 480 °C and 460 °C, respectively. The as-quenched samples and the samples annealed at a temperature lower than 450 °C are in the amorphous state. When they are annealed over the temperature range 490–600 °C, the nanocrystalline structure is formed, and the average grain size is about 20–40 nm. The further increase of the annealing temperature (above 600 °C) will cause the precipitation of Fe_3B (or Fe_3Zr) and growth of the grains. Typical x-ray diffraction patterns for $Fe_{73.5}CuNb_3Si_{13.5}B_9$ amorphous and crystallized states are shown in figure 1. The as-quenched sample consists only of a halo peak, revealing the formation of an amorphous phase. The broad peak changes to a (110) diffraction peak of a bcc structure on annealing above 480 °C (only the pattern for 550 °C is shown). Further heating to 650 °C causes the change of the bcc phase to mixed phases of α-Fe, Fe_3B, and other phases. This is consistent with results reported previously [16, 17].

3.2. Impedance spectra

The measurements of the impedance spectra for nanocrystalline samples indicate that the impedance $Z(f, H) = R(f, H) + iX(f, H)$ depends strongly on the frequency of the alternating drive current and the dc magnetic field. The magnetoresistance and magnetoreactance spectra of the $Fe_{88}Zr_7B_4Cu$ sample annealed for one hour at 545 °C with zero applied field and a field of 75 Oe are shown in figure 2. As shown in the figure, both the resistance and the reactance increased with frequency when the frequency increased above some critical value f^*. Being consistent with the skin effect, the value of f^* corresponds to the condition $a/\delta_m = 1$, where a and δ represent the thickness of the sample and the skin depth, respectively. At frequencies above f^*, the skin effect is

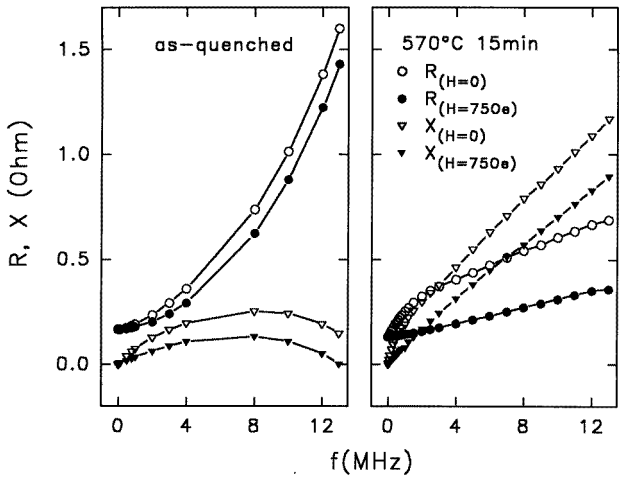

Figure 3. The dependence of the resistance R and reactance X on the drive ac frequency f for as-quenched and nanocrystalline $Fe_{73.5}CuNb_3Si_{13.5}B_9$ ribbons. The hollow dots represent the data obtained without an external field, and the black dots represent the data measured under a maximum dc magnetic field of 75 Oe in the longitudinal direction.

important. It can be noted in the figure that an applied magnetic field will move f^* to a higher frequency range. Under a 75 Oe field, the value of f^* for R is moved from 10 kHz to 1 MHz, and the value of f^* for X is moved from 5 kHz to 0.1 MHz. We infer that both the R- and X-spectra will tend to be flat if a larger field is applied. For the as-quenched sample, as shown in figure 2, the critical frequency f^* is quite high, being 8–9 MHz for R and 11 MHz for X, and the influence of the field of 75 Oe is too small to be detected. Since δ is proportional to $(\omega\mu)^{-1/2}$, where $\omega = 2\pi f$, and μ is the transverse permeability, a high f^* means a low permeability for the definite $\delta = a$ at the frequency $f = f^*$. This is consistent with the experimental results on effective permeability to be given in the following section.

Figure 3 shows the spectra of the magnetoresistance R and the magnetoreactance X of the as-quenched sample and the sample of $Fe_{73.5}CuNb_3Si_{13.5}B_9$ annealed at 570 °C. For the as-quenched sample, a striking feature that is mostly resistive over the whole frequency range is observed. As reported for Co-based amorphous ribbons, R has a positive curvature, while X shows a negative curvature versus frequency [9, 11]. This indicates that R would increase more and more sharply, while X would tend to saturation or would decrease. Thus this mostly resistive feature may be common to amorphous ribbon alloys. A remarkable feature of figure 3 contrasting with what is seen for amorphous samples is that X increases more sharply than R for the sample annealed at 570 °C. This indicates that for amorphous and nanocrystalline samples, different mechanisms dominate.

3.3. The annealing temperature dependence of the magnetoimpedance

The annealing temperature has a great influence on the magnetoimpedance of Fe-based ribbons. No GMI effect was observed if the ribbons were annealed at temperatures lower than the crystallizing temperature. A large MI effect was found in samples with fine nanocrystalline structure. The further increase of the annealing temperature (above 600 °C) will cause the precipitation of Fe_3B [16] (or Fe_3Zr [17]) and growth of the

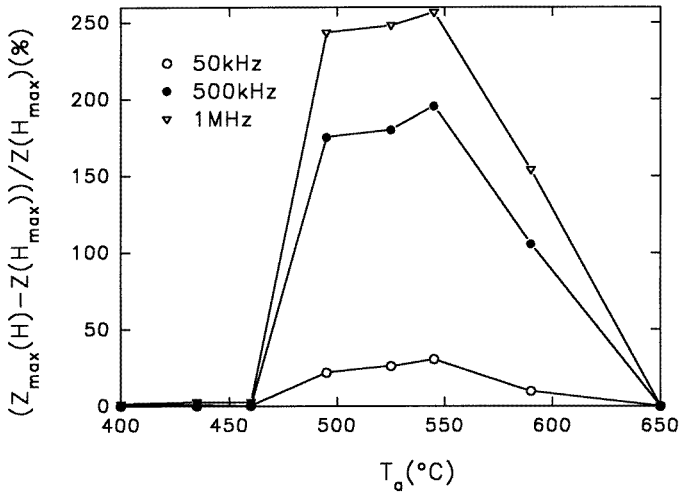

Figure 4. The annealing temperature dependence of the MI ratio for $Fe_{88}Zr_7B_4Cu$ ribbons, at the frequencies 50 kHz, 500 kHz, and 1 MHz.

grains. This will relieve the remaining inter-grain stress, and then eliminate the transverse magnetic anisotropy. Then the MI effect becomes very small due to the decreasing of the permeability. Figure 4 shows the annealing temperature dependence of the MI ratio $[Z_{max}(H) - Z(H_{max})]/Z(H_{max})$ for $Fe_{88}Zr_7B_4Cu$ samples at different frequencies, where $Z_{max}(H)$ is the maximum impedance value which will be shown in figure 6 (see later), and $Z(H_{max})$ is the impedance at $H_{max} = 75$ Oe. It is obvious that large MI effects occur for samples annealed at temperatures ranging from 490 °C to 600 °C.

3.4. The annealing time dependence of the impedance spectra

Figure 5 shows the MI spectra of the nanocrystalline $Fe_{73.5}CuNb_3Si_{13.5}B_9$ ribbons annealed at 550 °C for different lengths of time. The curve for the as-quenched sample is also given in figure 5 for comparison. When the frequency increases above the critical frequency f^*, the MI ratio $\Delta Z/Z = [Z(0) - Z(H_{max})]/Z(H_{max})$ increases quickly with increasing frequency, and reaches a maximum value $(\Delta Z/Z)_{max}$ at a characteristic frequency f_m. Then with the further increase of the frequency, $\Delta Z/Z$ decreases. The value of f^* is in the approximate range 10–30 kHz for nanocrystalline ribbons, and near 50 kHz for the as-quenched sample as figure 5 shows. The maximum magnetoimpedance $(\Delta Z/Z)_{max}$ increases first with the increasing of the annealing time T_a, and reaches the largest value at $T_a = 3$ h; then $(\Delta Z/Z)_{max}$ decreases slowly with the further increase of T_a. But the characteristic frequency f_m decreases first with the increasing of T_a, and then drops down to the lowest value at $T_a = 3$ h; subsequently, the value of f_m increases slightly with the further increase of T_a. The dependencies of f^*, f_m, and $(\Delta Z/Z)_{max}$ on the annealing time are summarized in figure 6. These dependencies of the parameters of the impedance spectra show that the magnetoimpedance of microcrystalline Fe-based ribbons are greatly affected by the annealing time too. By means of x-ray diffraction and permeability measurements, it was deduced that the proportion of crystalline volume and the size of the crystallized grains in a sample would augment with the increasing of the annealing time, and thus the decrease of the remaining longitudinal stress and the relative increase of the transverse

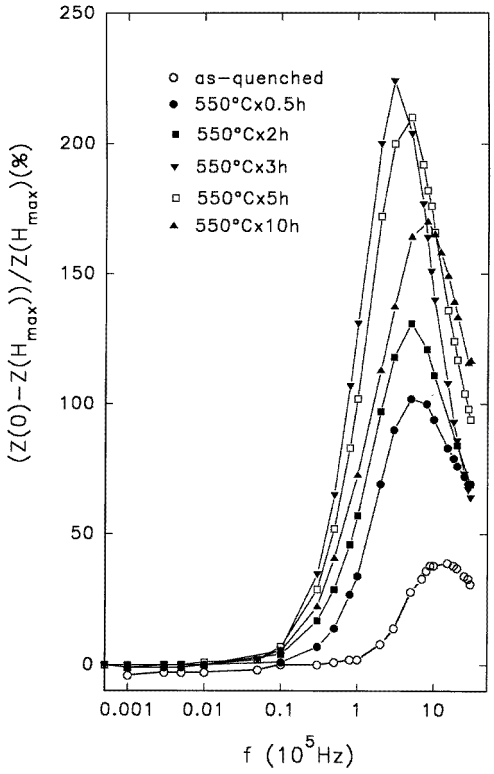

Figure 5. The dependence of the MI ratio on the drive alternating current frequency f for as-quenched amorphous and nanocrystalline $Fe_{73.5}CuNb_3Si_{13.5}B_9$ ribbons annealed for various times T_a.

stress would proceed accordingly. As a result, the permeability grows rapidly, and GMI is obtained. At $T_a = 3$ h, the sample was completely crystallized, with 20–30 nm grains, and a maximum MI ratio is obtained. But with the further increasing of T_a, the annealing makes the transverse stress decrease, and thus the permeability decreases accordingly. This makes the MI decline. No Fe_3B phase was observed with the annealing time increasing. The measured maximum value of $(\Delta Z/Z)_{max}$ is 227% for the sample annealed at 550 °C for 3 h under a 300 kHz drive current.

3.5. The field dependence of the impedance

Figure 7 shows the dependence on the magnetic field H of the MI ratio $\Delta Z/Z = [Z(H) - Z(H_{max})]/Z(H_{max})$ for $Fe_{73.5}CuNb_3Si_{13.5}B_9$ samples. For the as-quenched state, the MI declines slowly with the increasing of H, and no GMI can be observed. For the annealed state with nanocrystalline structure, the MI rises at first with the increasing of the applied magnetic field, and reaches a maximum which is located at about 7.2 Oe; then it decreases with the applied field. When a low longitudinal magnetic field is applied, the domains in which the moment directions are close to longitudinal will enlarge. Thus the transverse magnetic field produced by the alternating drive current will cause higher permeability. This then makes the MI rise with the longitudinal applied field. Once the applied field is higher than the anisotropy field, and makes all of the moments align along

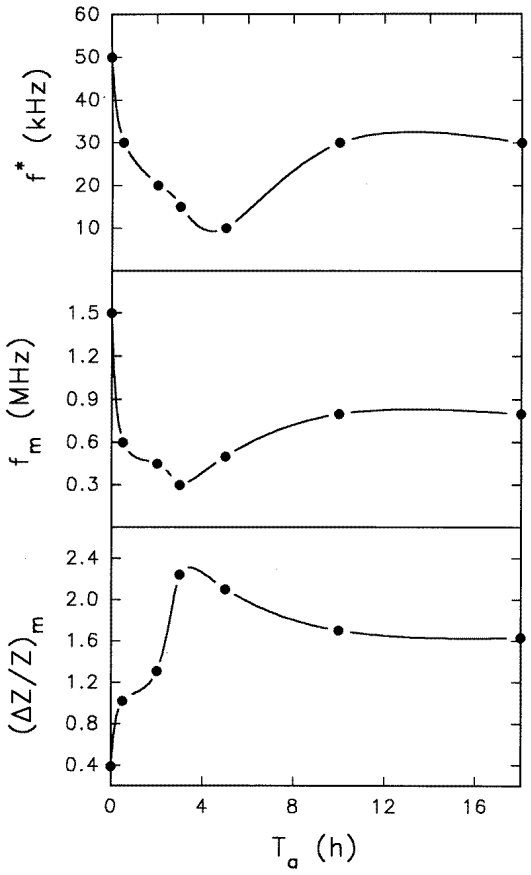

Figure 6. f^*, f_m, and $(\Delta Z/Z)_{max}$ as functions of the annealing time T_a.

the longitudinal direction of the samples, domain wall motion ceases to dominate. The transverse field produced by the alternating current is not high enough to take the place of the rotation process. Therefore, the MI is very low in the high-longitudinal-field range. The largest $\Delta Z/Z$ value is 435%, which was obtained for the samples annealed for 3–5 h at the frequency 800 kHz, and the sensitivity in the range of 3 Oe to 7.2 Oe is about 60% Oe^{-1}. Such an effect can be used in a number of technological applications, in magnetic sensors and magnetic recording devices. Under a periodic applied longitudinal field, the magnetoimpedance curves show a hysteresis effect. Figure 8 shows the hysteresis loops of the magnetoimpedance $Z(H, f) = R(H, f) + iX(H, f)$ for $Fe_{88}Zr_7B_4Cu$ samples. The range of the applied longitudinal field is from -75 Oe to 75 Oe. Two maximum peaks are located at around $+3.5$ Oe and -3.5 Oe respectively. The sub-minimum is at $H = 0$. The MI tends to saturation at 75 Oe. It can be seen that for MI its saturation field depends on the ac frequency: the higher the frequency, the larger the saturation magnetic field. The location of the MI peaks will move toward higher field slightly when a higher frequency is used. For $Fe_{88}Zr_7B_4Cu$, the value of $(\Delta Z/Z)_{max}$ is about 409% at 10 MHz. Compared with $Fe_{73.5}CuNb_3Si_{13.5}B_9$, $Fe_{88}Zr_7B_4Cu$ shows much better high-frequency characteristics. The behaviour of the MI–H relation mentioned above is identical to the behaviour that the Co-based amorphous wires with a circumferential magnetic anisotropy showed [1–4]. So it

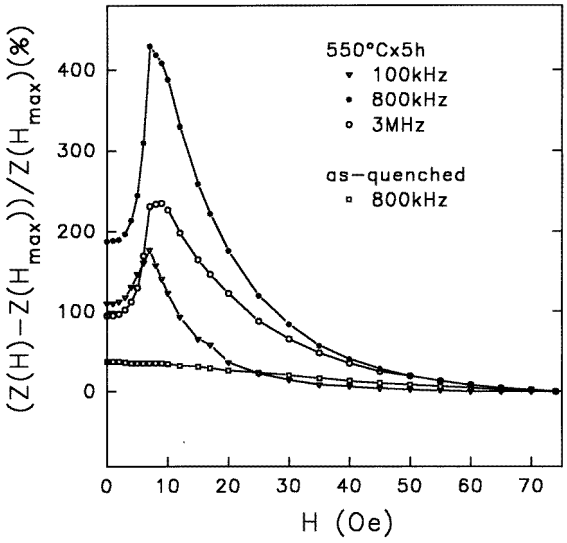

Figure 7. The MI ratio as a function of the applied dc magnetic field H for the as-quenched and the annealed nanocrystalline $Fe_{73.5}CuNb_3Si_{13.5}B_9$ ribbons.

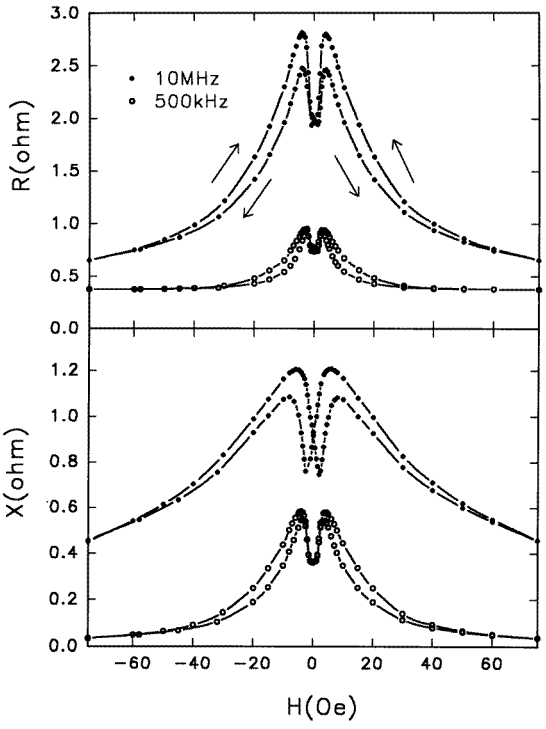

Figure 8. The dependences of the resistance and reactance of the $Fe_{88}Zr_7B_4Cu$ sample annealed for 1 h at 545 °C on the applied dc field H at the frequencies $f = 500$ kHz and 10 MHz.

can be suggested that a transverse magnetic anisotropy has been formed by natural annealing in the 500–600 °C range (the mechanism will be discussed in the following section). From figure 7 and figure 8, the transverse anisotropy fields H_k for $Fe_{73.5}CuNb_3Si_{13.5}B_9$ and $Fe_{88}Zr_7B_4Cu$ are about 7.2 Oe and 3.5 Oe respectively. When the applied longitudinal field $H < H_k$, the domain wall motion is dominant, but once $H > H_k$, the domain wall motion ceases, and the moment rotation process dominates; then the MI effect is reduced and saturated.

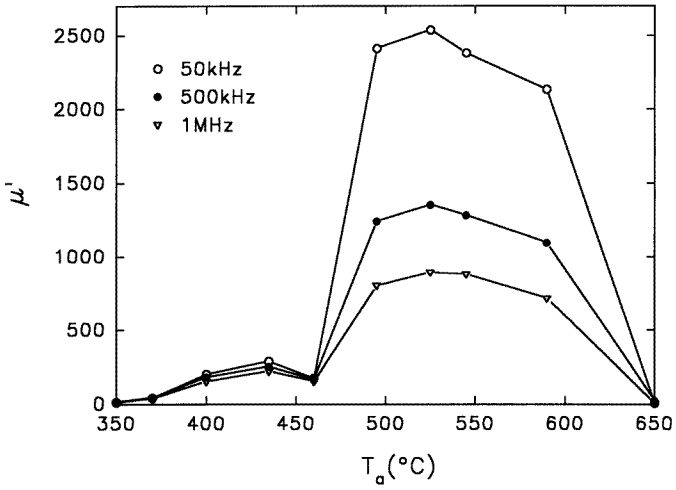

Figure 9. The annealing temperature dependence of the effective permeability μ' at the frequencies 50 kHz, 500 kHz, and 1 MHz.

3.6. The effective permeability

The effective permeability μ' of the as-quenched sample is small for the $Fe_{73.5}CuNb_3Si_{13.5}B_9$ composition ($\sim 10^2$), is very small for the $Fe_{88}Zr_7B_4Cu$ composition ($\sim 10^1$), and increases with the increasing annealing temperature to a very large value ($\sim 10^3$), and then drops rapidly, as shown in figure 9 for $Fe_{88}Zr_7B_4Cu$ ribbons. The pattern looks similar to figure 4. It is obvious that a large MI effect occurs for samples annealed at temperatures between 490 and 600 °C, when the nanocrystalline structure is formed and the excellent soft magnetic property is produced. One can conclude that the soft magnetic property provided the basis for the GMI effect, and the skin effect causes the GMI effect to occur. The frequency and the field dependences of μ' for all of the nanocrystalline samples possess similar properties. Figure 10 shows the frequency dependence of μ' for both nanocrystalline and as-quenched samples of $Fe_{73.5}CuNb_3Si_{13.5}B_9$. We can see that μ' decreases sharply in the low-frequency range (<2 MHz), and then reaches saturation in the high-frequency range, for the domain wall motion is strongly damped by eddy currents in the high-frequency range, and the corresponding μ' is greatly reduced, as shown in the figure. Figure 11 shows the field dependence of μ'. We find that for the nanocrystalline sample, μ' first decreases slowly, then drops dramatically at the transverse anisotropy field (about 7.2 Oe), and finally saturates. However, μ' for amorphous samples decreases slowly over the whole field range (0 to 75 Oe), showing the absence of the transverse magnetic anisotropy in the as-quenched sample. In nanocrystalline samples, a transverse magnetic anisotropy is

induced by annealing, as we will discuss later. So the peak in the $\Delta Z/Z$–H curves (figure 7) corresponds to the onset of the moment rotation at that field, when the magnetization is aligned longitudinally by an applied field higher than the transverse magnetic anisotropy field. By comparing figure 11 and figure 7, one can conclude that the presence of the transverse magnetic anisotropy is essential for the large MI effects, as Sommer and Chien have pointed out [12].

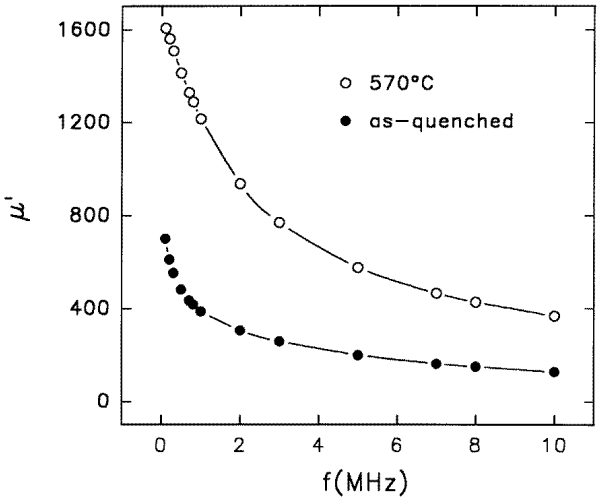

Figure 10. The dependence of the effective permeability μ' on the drive ac frequency f for the as-quenched and the nanocrystalline $Fe_{73.5}CuNb_3Si_{13.5}B_9$ ribbons.

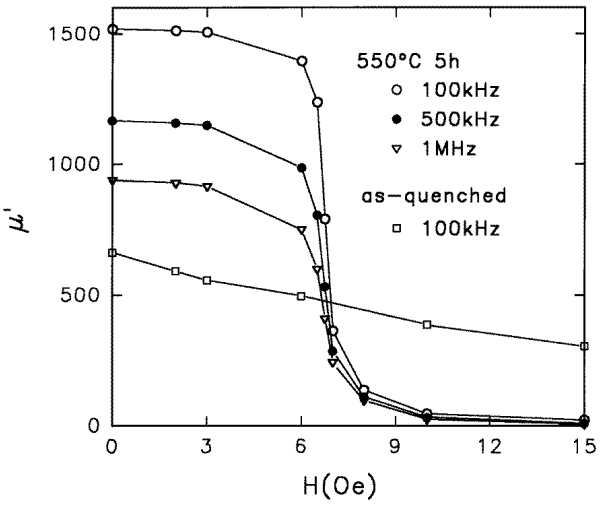

Figure 11. The dependence of the permeability μ' on the applied dc magnetic field H for the as-quenched and the nanocrystalline $Fe_{73.5}CuNb_3Si_{13.5}B_9$ ribbons at $f = 100$ kHz, 500 kHz, and 1 MHz.

3.7. The formation of the transverse anisotropy

It is generally believed that the anisotropy observed in amorphous ferromagnets is predominantly due to magnetostriction. Magnetostriction anisotropy is governed by the alloy composition, which determines the value of the magnetostriction constant λ, and stress fields, which result from the fabrication process. Amorphous ferromagnetic ribbons are produced by quenching a molten stream onto a water-cooled rotor. This process causes a longitudinally directed tensile stress formed in an as-quenched ribbon, and, consequently, a magnetic anisotropy that is either longitudinal or transverse, depending on the sign of λ.

Fe-based soft ferromagnet has a small positive value of λ, and this results in a longitudinal anisotropy field in the as-quenched state. When it is annealed naturally, the longitudinal tensile stress decreases; relatively speaking, the transverse stress increases. As a consequence, a transverse (or at least, one tending to be transverse) anisotropy arises. When it is annealed at an appropriate temperature and for an appropriate time, a fine transverse anisotropy can be formed, as we have seen for Fe-based nanocrystalline samples, above. In contrast, Co-based amorphous magnetic alloys such as $Fe_{4.3}Co_{68.2}Si_{12.5}B_{15}$ possess a slightly negative magnetostriction, of the order of -10^{-7}, so a transverse anisotropy exists in the as-quenched ribbons; annealing naturally will release the longitudinal stress, so the transverse magnetic anisotropy will decrease. We can see this clearly by comparing figure 8 above with figure 2 in reference [12]. The MI effects of Fe-based nanocrystalline samples show a property similar to that of the Co-based samples as-quenched or annealed with tensile stress (or a transverse field) [12]. The Fe-based as-quenched sample shows a property similar to that of Co-based samples annealed under a longitudinal magnetic field [12]. However, the magnitude of the MI ratio reported above is far larger than that for Co-based ribbons. Therefore, annealing at an appropriate temperature, without applying a transverse magnetic field or tensile stress, can result in a transverse anisotropy in Fe-based alloy ribbons and films. From the applications viewpoint, this technical characteristic is highly valuable in practice. The direct experimental verification of the formation of the transverse anisotropy is currently being undertaken.

In summary, the MI effects in amorphous and nanocrystalline $Fe_{73.5}CuNb_3Si_{13.5}B_9$ and $Fe_{88}Zr_7B_4Cu$ ribbons have been studied. We found that a GMI effect exists in nanocrystalline samples. A value of more than 400% for the MI ratio was obtained both for $Fe_{73.5}CuNb_3Si_{13.5}B_9$ and for $Fe_{88}Zr_7B_4Cu$ ribbons. The sensitivity can reach a value larger than 60% Oe^{-1} in a field range 3–7.2 Oe at 800 kHz for $Fe_{73.5}CuNb_3Si_{13.5}B_9$ ribbons. No GMI effect was observed in as-quenched amorphous $Fe_{88}Zr_7B_4Cu$ and $Fe_{73.5}CuNb_3Si_{13.5}B_9$ samples, because of their very low permeability, but a mostly resistive feature was found in as-quenched amorphous $Fe_{73.5}CuNb_3Si_{13.5}B_9$ samples. The field dependence of the effective permeability shows a typical transverse anisotropy property, and the formation of the transverse anisotropy in Fe-based ribbons annealed naturally was analysed. A detailed theoretical treatment of the results is under way.

Acknowledgments

This work was supported by the National Natural Science Foundation of China, the Doctoral Training Foundation of the National Education Commission of China, and the State Key Laboratory of Magnetism, Institute of Physics, Chinese Academy of Sciences.

References

[1] Mohri K, Kawashima K, Kohzawa T, Yoshida Y and Panina L V 1992 *IEEE Trans. Magn.* **28** 3150
[2] Mohri K, Kawashima K, Kohzawa T and Yoshida Y 1993 *IEEE Trans. Magn.* **29** 1245
[3] Panina L V and Mohri K 1994 *Appl. Phys. Lett.* **65** 1189
[4] Beach R S and Berkowitz A E 1994 *Appl. Phys. Lett.* **64** 3652
[5] Mandal K and Ghatak S K 1993 *Phys. Rev.* B **47** 14 233
[6] Machado F L A, da Silva B L, Rezende S M and Martins C S 1994 *J. Appl. Phys.* **75** 6563
[7] Velázquez J, Velázquez M, Chen D X and Hernando A 1994 *Phys. Rev.* B **50** 16 737
[8] Rao K V, Humphrey F B and Costa-Krämer J L 1994 *J. Appl. Phys.* **76** 6204
[9] Machado F L A, Martins C S and Rezende S M 1995 *Phys. Rev.* B **51** 3926
[10] Panina L V, Mohri K, Uchiyama T and Noda M 1995 *IEEE Trans. Magn.* **31** 1249
[11] Beach R S and Berkowitz A E 1994 *J. Appl. Phys.* **76** 6209
[12] Sommer R L and Chien C L 1995 *Appl. Phys. Lett.* **67** 857
[13] Chen C, Luan K Z, Liu Y H, Mei L M, Guo H Q, Shen B G and Zhao J G 1996 *Phys. Rev.* B **54** 6092
[14] Beach R S, Smith N, Platt C L, Jeffers F and Berkowitz A E 1996 *Appl. Phys. Lett.* **68** 2753
[15] Sommer R L and Chien C L 1995 *Appl. Phys. Lett.* **67** 3346
[16] Yoshizawa Y, Oguma S and Yamanchi K 1988 *J. Appl. Phys.* **64** 6044
[17] Suzuki K, Kataoka N, Inoue A, Makino A and Masumoto T 1990 *Mater. Trans. Japan Inst. Met.* **32** 743